Rate Loop Control Based on Torque Compensation in Anti-backlash Geared Servo System

Y.S. Kwon, H.Y. Hwang, H.R. Lee, and S.H. Kim

Abstract –**This paper proposes the methods that convert two nonlinear characteristics into linear ones in anti-backlash geared servo system. The method to linearize the nonlinear stiffness of the anti-backlash geared train is suggested by investigating the frequency response characteristics. For the purpose of eliminating the nonlinear friction, a new non-model based torque compensator is applied to the servo system. The friction increased by the anti-backlash gear train is measured using torque equation in steady state. The design guideline of this compensator to guarantee the stability is established by describing function analysis and R-H method. In the end, the performance of designed controller is demonstrated by the results of simulation and experiment both in the frequency and in the time domain.**

I. INTRODUCTION

A servo system using low power DC motor generally adopts a gear train structure in order to generate high torque. Unfortunately, the geared servo system shows undesirable nonlinear characteristic such as the backlash. This backlash characteristic reduces the effective stiffness of the gear train and eventually reduces the system bandwidth limited by the anti-resonance frequency[1][7]. To surmount the drawback, the anti-backlash gear mechanism has been introduced. Its mechanical structure improves the effective stiffness of the total gear train, and moves the anti-resonance and resonance frequencies to the higher ones. However, the anti-backlash gear train has more friction than the gear train with backlash not only because the contact area between drive and driven gears is increased, but also because the parallelism between gears is degraded by the initial twisting torque of the anti-backlash spring. The friction results in the tracking error of rate control loop, and eventually, it makes it difficult to design a high gain stabilization loop or a high-precision position control loop. A number of methods for friction compensation have been proposed in various research reports. Proposed methods are largely divided into a non-model-based compensation and a model-based one. The former methods have been presented as: stiff PD position control; integral control with a small dead band; dither control; impulse control; joint torque control, and dual mode control. The latter methods have been introduced as follows: Coulomb friction feedforward /back control; general friction feedforward/back control, and adaptive feedforward/back control[2]. Both of these methods have provided the various solutions to eliminate the friction in the field of industry and military. However, in case of the model-based compensators, they have to utilize not only the exact model identification for the friction, but also the adaptive algorithm based on programmable digital controller. Also, in case of a few non-model-based compensators, they are apt to have the additional defects such as the unstable self-oscillation, or extra power consumption in the steady state because they use the indirect compensation scheme different from methods mentioned previously.

This paper proposes the methods, which remove two nonlinear components in the anti-backlash geared servo system, so as to obtain a linearized speed control loop. First, the nonlinear stiffness of the anti-backlash gear train is linearized by selecting the proportional gain of the rate loop properly according to the anti-resonance frequency of the plant. Second, the nonlinear friction of this system is removed by using a new non-model-based compensator directly compensating the friction torque with the measured loss torque. The friction model in this simulation is expressed in the form of Karnopp model whose parameters are obtained from TEE. The stability according to the proportional controller gain and the proposed friction compensator is investigated by Routh's stability criterion and a describing function analysis[3][4]. Finally, the simulation results to step input command, sinusoidal tracking command, and frequency response are compared with experimental ones. The performance of the proposed compensator is demonstrated.

II. SYSTEM IDENTIFICATION

A. Friction model for simulation

Generally, a classical friction torque is defined as the function of a velocity,

$$T_f(\theta) = T_c sign(\dot{\theta}) + T_v \dot{\theta} \qquad (1)$$

Manuscript received January 26,2004. This work was supported in part by LG Innotek Company, Ltd.

Y.S. Kwon, H.R. Lee, and S.H. Kim are with R&D, LG Innotek Co.,Ltd. 148-1, Maburi, Guseong-eup, Yongin-city, Kyonggi-do, 449-910, Korea (Tel:+82-31-288-9302; e-mail: yskwon@lginnotek.com)

Hong Yeon Hwang is with Technical R&D Center, Agency For Defense Development, Yuseong P.O.BOX 35-4 Taejon, 305-600, Korea (Tel : +82-42-821-4464; e-mail: hyhwang@add.re.kr)

where T_c is the Coulomb friction torque and T_v is the viscous friction coefficient. When the rate is zero, the above model can be described in more detail by adding the following sticking model, which is expressed in terms of the external torque:

$$T_{stick} = \begin{cases} T_e, & |T_e| < T_s, \quad \dot{\theta} = 0, \quad \ddot{\theta} = 0 \\ T_s \operatorname{sgn}(T_e), & |T_e| \geq T_s, \quad \dot{\theta} = 0, \quad \ddot{\theta} \neq 0 \end{cases} \tag{2}$$

where T_e is the external torque and T_s is the breakaway torque. If (2) is combined with (1), the classic static model is completed as (3).

$$T_f = \begin{cases} T_f(\dot{\theta}), & \dot{\theta} \neq 0 \\ T_e, & |T_e| < T_s, \quad \dot{\theta} = 0, \quad \ddot{\theta} = 0 \\ T_s \operatorname{sgn}(T_e), & |T_e| \geq T_s, \quad \dot{\theta} = 0, \quad \ddot{\theta} \neq 0 \end{cases} \tag{3}$$

where $T_f(\dot{\theta})$ is an arbitrary function. According to (3), the static model cannot be depicted as a function of velocity only. The classical friction factors can be discontinuously combined as shown in Fig.1a. However, the discontinuity between breakaway and Coulomb friction torque level can be described as a continuous function of the velocity, which is called Stribeck curve, as shown in Fig.1b [5].

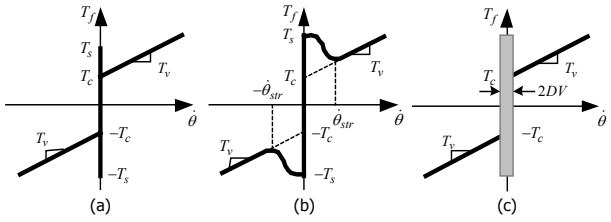

Fig.1(a) discontinuity model, (b) Stribeck model, (c) Karnopp model

The nonlinear function using the Stribeck curve is:

$$T_f(\dot{\theta}) = \left[T_c + (T_s - T_c) \exp\left(- \left| \dot{\theta} / \dot{\theta}_{str} \right|^2 \right) \right] \operatorname{sgn}(\dot{\theta}) + T_v \dot{\theta} \tag{4}$$

where $\dot{\theta}_{str}$ is called the Stribeck velocity. When the velocity is zero, the above model does not clearly distinguish the region of zero speed. Consequently, there is a difficulty for simulation or control usage. A simulation method for solving this difficulty was introduced by Karnopp[6]. This model defines the stick-slip area as a zero velocity interval so as to avoid the switching between sticking and sliding as shown in Fig.1c.

B. Friction parameter identification

In order to identify the friction torque parameters, the torque equilibrium relationship in the steady state is applied. Torque equilibrium means that an applied torque is equal to a friction torque when the rate of the inertia system keeps a constant without any acceleration [1][5].

$$T_{app} = J\ddot{\theta}_m + T_f \quad \Rightarrow \quad T_{app} = T_f \tag{5}$$

where T_{app} is an applied torque and $\ddot{\theta}_m$ is the motor acceleration. The friction parameters can be identified based on the relationship between the applied torque and the steady state speed for various step input commands.

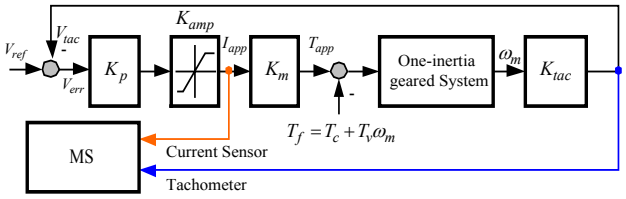

Fig.2 Estimation of disturbance torque

A current sensor and a tachometer expressed in Fig.2 are used for measuring the applied torque and the motor speed, respectively. Equation (6) presents that it is possible to identify the Coulomb torque and viscous coefficient by using measured value from the sensors.

$$T_{app} = T_f \Leftrightarrow I_{app} \cdot K_m = T_c + T_v \left(\frac{V_{tac}}{K_{tac}} \right) \tag{6}$$

where I_{app} is the applied current, K_m is the torque coefficient of motor, K_{tac} is the tachometer sensitivity, V_{tac} is the output volt of the tachometer, and *MS* denote a measuring system.

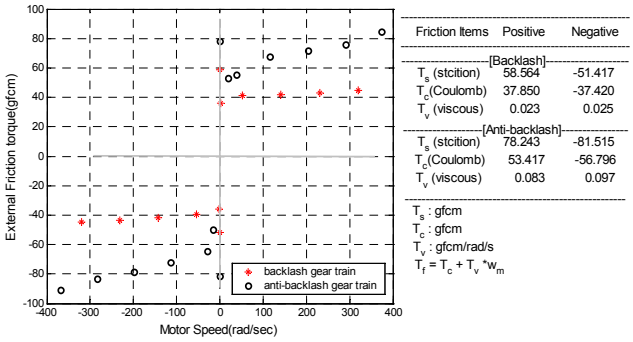

Fig.3 Friction torque of backlash and anti-backlash

The experimental results shown in Fig.3 make it possible to find not only the relationship between friction torque and motor speed, but also the fact that the anti-backlash geared system has more friction than the backlash geared system. The right side of Fig.3 shows the friction parameters identified by the least square method.

C. Anti-backlash gear train structure

A geared mechanism increases the final output torque proportional to the gear ratio but inevitably causes the backlash that degrades the accuracy of the position. The resonance and anti-resonance frequencies of the geared servo system depend on both the backlash angle and the motor input voltage[7]. These frequencies restrict the freedom to design a desirable control loop. The less the backlash is, the easier the control loop design is, because these resonance and anti-resonance frequencies become higher. In order to reduce the gear backlash, anti-backlash gear mechanism is introduced, where a torsion spring bar is inserted inside a pair of gear and it acts as a spring torque

to remove the backlash. The anti-backlash gear set shown in Fig.4a is assembled with pinion gear after that the free wheel gear is rotated by the amount of initial turn torque so as to remove the backlash effect. As shown in Fig.4b, the stiffness of the gear train is equivalent to zero backlash case when the motor rotates in one direction. On the other hand, when the motor rotates in the opposite direction, the stiffness becomes equivalent to zero backlash case after the anti-backlash spring is perfectly compressed and does not have the elastic torque any more. This kind of gear structure makes it possible to control to increase the resonance and anti-resonance frequencies, which limit the bandwidth of the servo system, by the enhanced effective stiffness of the gear train.

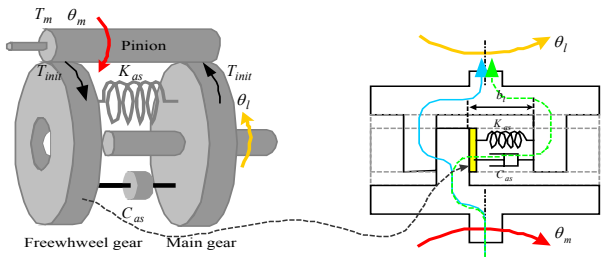

(a) Anti-backlash installation (b) Torque path

Fig. 4 Schematic of anti-backlash gear train

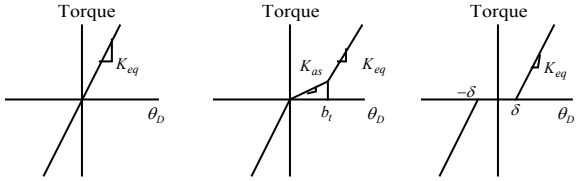

(a) without backlash (b) anti-backlash (c) backlash

Fig.5 Stiffness to transmission angle error

Fig.5b implies that the larger the transmission angle error, θ_D, between drive and driven shaft is, the stiffer the gear train is for the positive direction. In other words, the input voltage of motor affects the total stiffness of the gear train as long as the backlash angle is invariant. This shows the same phenomenon as the backlash gear train has [7]. If the input is $\theta_D \sin \omega t$, the gain of the normalized describing function gain for the backlash model shown in Fig.5c is given as:

$$N(\theta_D) = \frac{2}{\pi}\left[\frac{\pi}{2} - \sin^{-1}\left(\frac{\delta}{\theta_D}\right) - \frac{\delta}{\theta_D}\sqrt{1-\left(\frac{\delta}{\theta_D}\right)^2}\right] \qquad (7)$$

where δ is $b_t/2$ and b_t is the total backlash. Moreover, since the amplitude θ_D can take $0 \le \theta_D < \infty$, the gain $N(\theta_D)$ has $0 \le N(\theta_D) < 1$, and the effective torsion stiffness reduced by the backlash can be expressed as:

$$K_{eff} = N(\theta_D) \cdot K_{eq} \qquad (8)$$

where K_{eq} is the total equivalent torsion stiffness of the gear train(*gfcm/rad*) with zero backlash. However, it is impossible to derive the describing function for the anti-backlash gear train because of it's asymmetric characteristic. Therefore, the effective torsion stiffness of the anti-backlash gear train is presumed using Fig. 5b and (8) as following manner:

$$K_a = \alpha \cdot K_{eq}, \qquad [\, N(\theta_D) < \alpha < 1\,] \quad (9)$$

where K_a is the torsion stiffness of the anti-backlash gear train.

D. Two-inertia system model with friction

Fig.6 shows an anti-backlash geared servo system consisting of the digital controller and the current amp to drive the motor. Since this system has five-inertia structure, it is not easy to formulate the plant characteristic analytically. Assuming that the inertia of the gear train is negligible enough compared with the motor and load inertias, the above system can be simplified as a two-inertia system shown in Fig.7. The proposed two-inertia model has the inherent features enough to reveal the distinctive characteristics that the five-inertia system has.

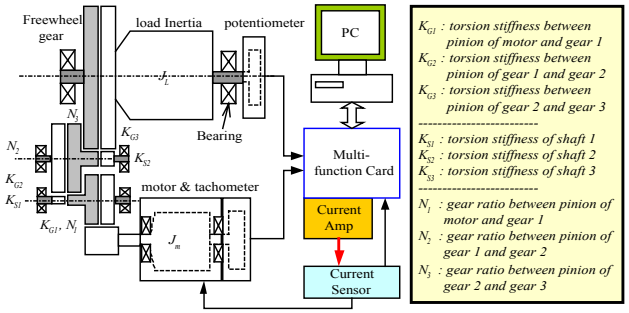

Fig.6 The structure of anti-backlash geared servo system

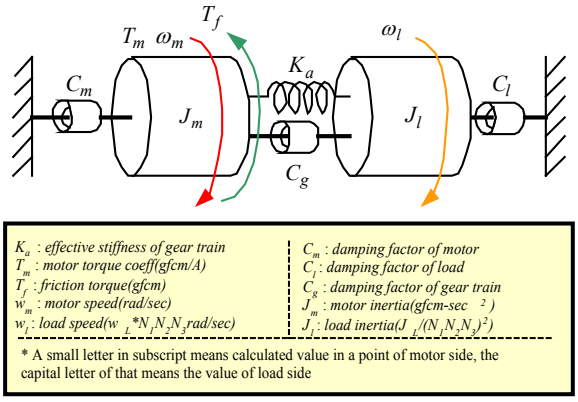

Fig.7 The model of anti-backlash geared servo system

The total torsional stiffness of the gear train without backlash is calculated by considering several factors such as Lewis form factor for gear teeth, elastic deformation factor for gear teeth, modulus of elasticity of the gear material, pitch diameter of gear, the tooth face of gear, the shear modulus of elasticity of the shaft, (10), and (11) [8].

$$K_1 = \frac{K_{G1}K_{S1}}{K_{G1}+K_{S1}}, \quad K_2 = \frac{K_{G2}K_{S2}}{K_{G2}+K_{S2}}, \quad K_3 = K_{G3} \qquad (10)$$

$$K_{eq} = \frac{(N_2N_3)^2 K_1K_2K_3}{K_2K_3 + N_3^2K_1K_3 + (N_2N_3)^2K_1K_2} \qquad (11)$$

where K_1 is the equivalent torsional stiffness of gear1

and rotating shaft1 (gfcm/rad), K_2 is the equivalent torsional stiffness of gear2 and rotating shaft2, and K_3 is the equivalent torsional stiffness of gear3.

Assuming that the stiffness of system does not change and keeps a constant for a large enough input voltage of the motor, we can utilize the describing function for Coulomb friction so as to obtain the transfer function between input torque and motor speed. The normalized describing function for the relay-type nonlinearity is presented as following equation [3]:

$$N(X) = \frac{4}{\pi X} \tag{12}$$

where X is the input amplitude. The friction torque to a sinusoidal input can be depicted as following equation:

$$T_f(\omega_m) = T_v\omega_m + T_c N(X)\omega_m \tag{13}$$

Also assuming that the influence of damping coefficients C_m, C_l, and C_g on the system are relatively small compared with that of the stiffness term, the transfer function between ω_m and T_m for the two-inertia system in Fig.7 can be obtained as follows.

$$\frac{\omega_m}{T_m} = \frac{(J_l s^2 + K_a)}{J_m J_l s^3 + J_l T_f s^2 + K_a(J_m + J_l)s + K_a T_f} \tag{14}$$

The frequencies corresponding to zeros and poles of this transfer function are called anti-resonance and resonance frequencies, respectively, and the anti-resonance frequency can be easily written by the effective stiffness and the load inertia as shown in (15). It is difficult to obtain the exact formulation for the resonance frequency because the resonance frequency depends on the effective stiffness as well as the friction torque.

$$f_{AR} = \frac{1}{2\pi}\sqrt{\frac{K_a}{J_l}} \tag{15}$$

The frequency responses for the backlash and the anti-backlash gear trains are examined by using a negative feedback with unit gain proportional controller presented in Fig.8. The effective stiffness for two types of gear train in the two-inertia system can be estimated from (15).

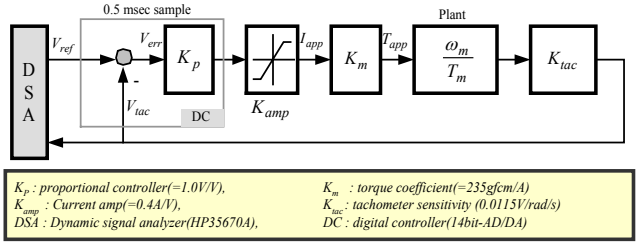

Fig.8 Experimental setup for frequency response

The Bode plots in Fig.9a and 9b show that the effective stiffness for both backlash and anti-backlash geared systems is distinctively changed according to the input voltage of motor. However, if the gain of the proportional controller is designed properly, the effective stiffness of the anti-backlash geared system coincides with that of the geared system with no backlash. Also, this result implies that when the motor input voltage is greater than 4.0V, the nonlinearity of the anti-backlash gear train can be neglected, and analytical stiffness can be used in this servo system.

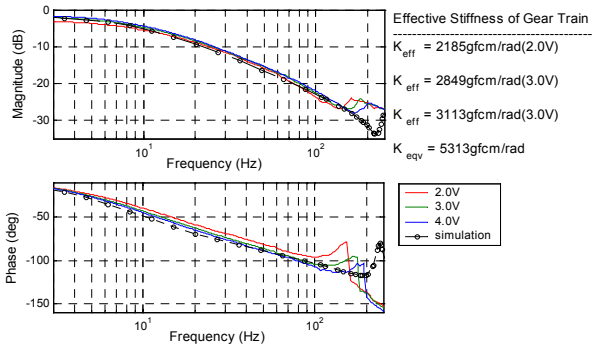

Fig.9a Frequency response of backlash gear train

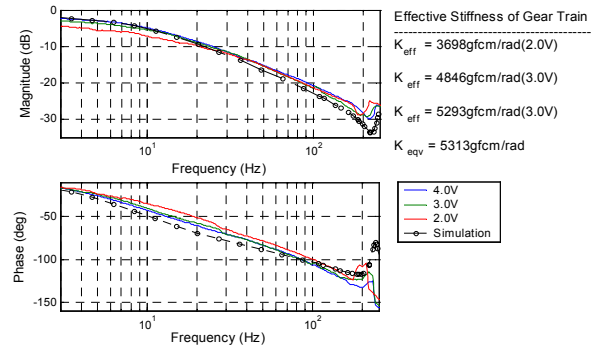

Fig.9b Frequency response of anti-backlash gear train

III. FRICTION COMPENSATION

The friction compensator proposed in this paper can overcome the sticking friction by a double-gain effect of the basic proportional controller when the motor speed is zero, and also the dynamic friction by compensating the loss torque when the motor is spinning. The loss torque is the error between the applied and the actual torques. The applied torque is calculated by measuring the motor current, and the actual torque is estimated from the product of the total inertia and angular acceleration, which is the differentiated value of the tachometer output. This sensor-based technique allows the compensator has advantages of both the model-based method compensating the friction directly and the non-model-based method not using the friction model.

A. Limit cycle analysis for friction compensation

Before applying the friction compensator, the existence of the limit cycle in the closed-loop system must be analyzed based on the describing function. Fig.10 depicts the block diagram of the closed-loop servo system with the proportional controller and the proposed friction compensator. The plant friction is expressed by the static Coulomb friction model written by (1). The total inertia of

the system is numerically calculated using IDEAS program. Although any filters are not shown in this figure, the low pass filters, which have high cut-off frequencies and do not affect the system bandwidth, are actually included to suppress the undesirable sensor noise.

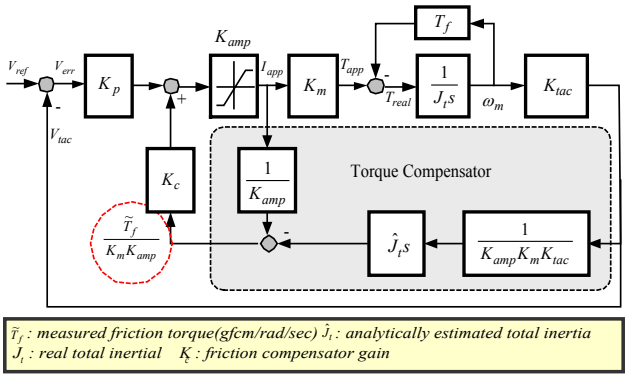

Fig.10 Block diagram of servo system with friction compensation and proportional controller

To test the existence of the limit cycle, the describing function for relay-type nonlinearity is used as described in (12). The transfer function of the above closed-loop system is derived as the following equation:

$$\frac{\omega_m}{V_{ref}} = \frac{K_p K_{amp} K_m}{J_t s + K_p K_{amp} K_m K_{tac} + \Delta T_v + \Delta T_c N(X)} \quad (16)$$

where ΔT_v is $T_v - K_c \tilde{T}_v$ and ΔT_c is $T_c - K_c \tilde{T}_c$ .The characteristic equation of this transfer function is:

$$J_t s + K_p K_{amp} K_m K_{tac} + \Delta T_v + \Delta T_c N(X) = 0 \quad (17)$$

The characteristic equation can be divided into a nonlinear part and a linear one to apply an extended Nyquist criterion as the following equation:

$$-\frac{1}{N(X)} = \frac{\Delta T_c}{J_t s + K_p K_{amp} K_m K_{tac} + \Delta T_v} = G_L(j\omega) \quad (18)$$

When equation (18) is satisfied for a specific sinusoidal function with arbitrary amplitude X and oscillation frequency ω, the limit cycle behavior will occur. To find these frequencies and amplitudes, equation (18) can be separated into real and imaginary parts as follows:

$$\mathrm{Re}\{G_L\} = \frac{\Delta T_c (K_p K_{amp} K_m K_{tac} + \Delta T_v)}{(K_p K_{amp} K_m K_{tac} + \Delta T_v)^2 + J_t^2 \omega^2} \quad (19)$$

$$\mathrm{Im}\{G_L\} = \frac{J_t \Delta T_c \omega}{(K_p K_{amp} K_m K_{tac} + \Delta T_v)^2 + J_t^2 \omega^2} \quad (20)$$

Using (12), (18), (19), and (20), the amplitude and frequency for the limit cycle are obtained as follows:

$$X_{LC} = -\frac{4}{\pi} \frac{(T_c - K_c \tilde{T}_c)}{(K_p K_{amp} K_m K_{tac} + \Delta T_v)}, \quad \omega_{LC} = 0 \quad (21)$$

From (21), if the compensation torque is larger than the actual friction torque in a steady state, the right side term of this equation becomes positive, and this system has the possibility to generate the limit cycle phenomenon because the amplitude, X_{LC} , is always positive. Additionally, if we describe the one-inertia model of Fig.10 as the two-inertia model, there are two limit cycle frequencies in this system. The one occurs in the same frequency as the one-inertia system, and the other occurs in the resonance frequency. However, herein, we do not consider the limit cycle in the resonance frequency because it exists out of control scope.

B. Stability of system

The limit cycle due to the nonlinear element and the insufficient stability margin makes the system unstable. To avoid the self-oscillation by the limit cycle, the real friction should always be greater than the compensating friction. The closed-loop system without the nonlinear component such as Coulomb friction will be stable if and only if

$$K_p K_{amp} K_m K_{tac} + \Delta T_v > 0 \quad (22)$$

Moreover, the proportional gain K_p must be sufficiently large in order to eliminate the nonlinear effect due to the backlash. Table.1 shows the design guideline for the servo system with proportional gain controller and friction compensator.

Table 1. Stability guideline

	$\Delta T_v > 0$	$\Delta T_v < 0$
$\Delta T_c > 0$	Always stable	$K_p > -\Delta T_v / (K_{amp} K_m K_{tac})$
$\Delta T_c < 0$	Always unstable	$K_p < -\Delta T_v / (K_{amp} K_m K_{tac})$

IV. SIMULATION AND EXPERIMENT RESULTS

The simulation was performed using Karnopp computer simulation method, and the experiments were performed using dynamic signal analyzer(HP3560A), multi-function board (APCI-3120), Howland current pump type amp made by LGIT, Axsys servo motor with tachometer(MT1300-XX-XX), current sensor(CLN-25:F.W. Bell), PIII computer, and LabView6.0.

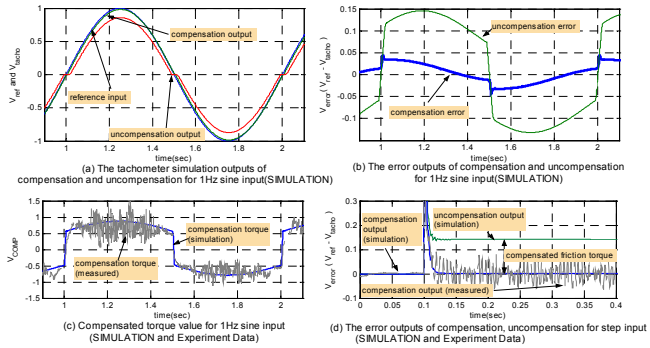

Fig.11 Simulation and experimental data for sinusoidal and step input

The simulation results for the compensated and the uncompensated system for 1V(1Hz) sine input depict that the compensator eliminates the dynamic friction and the break away torque practically in Fig.11a. The compensated error is very small compared with the uncompensated one,

as shown in Fig.11b, and the compensating torque well coincides with that by simulation in Fig.11c. The difference between compensated and uncompensated system shown in Fig.11d explains that the compensator to a step input rewards the loss torque by friction. Fig12a shows two kinds of responses for a sine input. The experimental data for a sinusoidal response presented in both Fig.12b and Fig.12c demonstrate that the sticking torque is nearly removed by double-gain effect of the proposed controller, and also that the dynamic friction is eliminated by the torque compensator. In summary, a compensated system can well track the sinusoidal command compared with the uncompensated case.

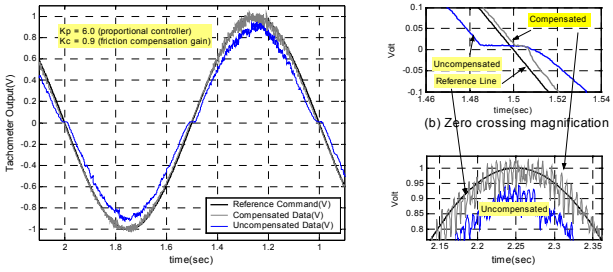

(a) Response for sinusoidal input command (b) Zero crossing magnification (c) Amplitude magnification

Fig.12 Experimental data of compensated and uncompensated system for 1.0V(1.0Hz) sinusoidal input command

Fig.13a shows the step responses according to gain of compensator, and as the gain approaches unit, there is no friction torque effect in this system. Also, Fig.13b shows that there exists a limit cycle when the delta friction has a negative value. In fact, we can achieve the similar performance by adding an integral term to the proportional controller, but on the contrary, the phase delay increases and the performance is degraded when the controller is used as an inner loop controller.

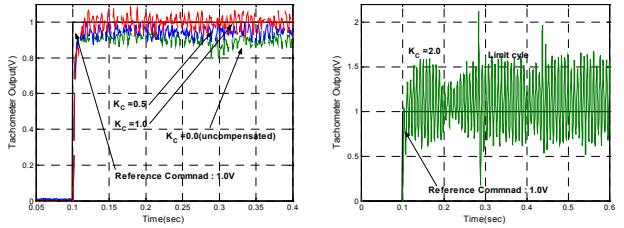

(a) Step response according to compensator gain K_c (b) Limit cycle phenomenon for over gain(K_c >1.0)

Fig.13 Experimental data of compensated and uncompensated system for step input command

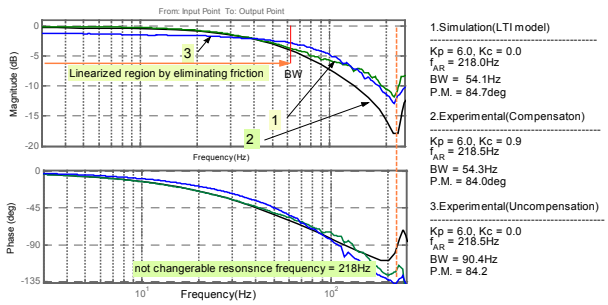

Fig.14 Bode Plot for compensated real system, uncompensated real system, and uncompensated linear model without friction

The responses for three types of systems in Fig.14 show that the frequency response of the linear time-invariant system model, where LTI viewer in MatLab can't express the behavior of the nonlinear element, matches well with the friction compensated system in the lower frequency region than the bandwidth frequency, but the shape of frequency response in the higher frequency region than the bandwidth is little bit different from the compensated system. In conclusion, these results explain that the friction compensated system can be utilized as a linear system under the bandwidth frequency. It is also found that the friction of the uncompensated system decreases the DC gain of the system, but increases the bandwidth.

V. CONCLUSION

This paper introduces the behavior of anti-backlash gear, and proposes a method to eliminate the nonlinearity of the anti-backlash gear by means of sufficiently large proportional gain in two-inertia system. To remove the increased friction due to employing the anti-backlash gear as a power transmission, a new non-model-based method that rids the servo system of the dynamic friction torque was presented using a current sensor and a tachometer. The stability of the system with the friction compensator was examined by describing function analysis including expanded Nyquist criterion. Also, the performances of the designed compensator were compared with those by the simulation model results having the Karnopp friction structure. The experimental results of the actual plant with PC based digital controller were analyzed for sinusoidal, step input, and frequency response. The experimental results demonstrated the adaptive peculiarities for instantly variable dynamic friction.

VI. REFERNCES

[1] Y. S. Kwon, H. Y. Hwang, "Stabilization Loop Design Method on Dynamic Platform", *ICASS2001*, Jeju, Korea, 2001.

[2] Armstrong-Helouvry, "A Survey of Models Analysis tools and Compensation Methods for the Control of Machines with Friction", *Automatica*, vol.30(7), 1994, pp.1083-1138.

[3] Jean-Jacques E. Slotine, *Applied Nonlinear Control*, Prentice-Hall, pp.157-190.

[4] Gene F.Franklin, *Feedback Control of dynamic systems, 2nd*, Addison Wesley, pp138-143.

[5] Olsson, H., et al., "Friction Models and Friction Compensation", *J. of Europ.Control*, vol.4(3), 1998.

[6] Dean Karnopp, "Computer simulation of Stick-Slip Friction in Mechanical Dynamic systems", *Transactions of the ASME*, vol.107, pp.100-103, March 1985.

[7] J. H. Beak, "Analysis on the Influence of Backlash and Motor Input voltage in Geared servo system", *IEEE2003, Mediterranean Conference on Control and Automation*, Rehodes, Greece, 2003.

[8] Bruce A. Chubb, *Modern Analytical Design of Instrument Servo Mechanisms*, Addison Wesley, 1967, pp.35-44.